EFLAM: A MODEL TO LEVEL-LINE JUNCTION EXTRACTION

N. Suvonvorn
Institut d'Electronique Fondamentale, Université Paris 11
Bâtiment 220 - 91405 Orsay Cedex
Email: nikom.suvonvorn@ief.u-psud.fr

B. Y. Zavidovique
Institut d'Electronique Fondamentale, Université Paris 11
Bâtiment 220 - 91405 Orsay Cedex
Email: bertrand.zavidovique@ief.u-psud.fr

Keywords: Level-line, level sets, corner, point of interest, extraction.

Abstract: This paper describes an efficient approach for the detection of level-line junctions in images. Potential junctions are exhibited independent from noise by their consistent local level-variation. Then, level-lines are tracked through junctions in descending the *level-line flow*. Flow junctions are extracted as image primitives to support matching in many applications. The primitive is robust against contrast changes and noise. It is easily made rotation invariant. As far as the image content allows, the spread of junctions can be controlled for even spatial distribution. We show some results and compare with the Harris detector.

1 INTRODUCTION

Image matching is a fundamental step for many applications such as stereovision, motion analysis and object recognition. This paper describes an image feature peculiarly suitable for matching, and its extraction. The feature is based on local topology of the image and is defined by simple mathematical morphology : that is the level-line junction. It is rotation invariant and especially robust to contrast changes (Monasse and Guichard, 1998). We explain how to extract the reliable feature by introducing the level-line flow and then the flow junction. A novel intensity variation detector is derived from there to enhance potential level-line junctions. The operator can be considered an extension of the SUSAN method (Smith and Brady, 1997) improved to detecting intensity variations around level-line junctions. It is inspired by the quite older Girard's detector (Girard, 1980) and from the work later by Bonnin (Bonnin et al., 1989). The paper is organised as follows : in section 2 we present the level-line flow and its junctons, the section 3 explains how to detect the potential flow junctions, then we detail the extraction algorithm and we define the related image feature in section 4. Eventually results are discussed and comparisons made in the last section.

2 LEVEL-LINE FLOW AND FLOW JUNCTIONS

Most signal processing would analyse a signal by decomposing it onto basic objects through basic operations. For example, a Fourier transform will decompose the signal into a sum of sin and cosin elementary signals - i.e. different frequencies - based on the inner product. However in case of natural images where contrast changes are significant the method is not well adapted. $I = I_1 + I_2$ does not mean that $g(I) = g(I_1) + g(I_2)$, when g is non-linear as most contrast models are. Other classical methods decompose images for instance into edges and regions to be combined in a non additive fashion too. Again, many such methods are very sensitive to contrast changes.

For our method to be robust to contrast changes we decompose the image into its *level sets* (Caselles et al., 1999), that is to say a morphological variable. Let $I(\mathrm{p})$ be the image intensity at pixel p and $\widetilde{I}(\mathrm{p})$ the result of the decomposition into level sets. A level set is defined as: (1) upper level set $N^s_\lambda = \{\mathrm{p}/I(\mathrm{p}) \geq \lambda\}$, (2) lower level set $N^i_\lambda = \{\mathrm{p}/I(\mathrm{p}) \leq \lambda\}$. Level sets contain all information needed for the image reconstruction. I is recovered from $I(\mathrm{p}) = \mathbb{O}[\widetilde{I}(\mathrm{p})] = sup\,\{\lambda/\mathrm{p} \in N^s_\lambda\}$ or equivalently from $I(\mathrm{p}) = \mathbb{T}[\widetilde{I}(\mathrm{p})] = inf\,\left\{\lambda/\mathrm{p} \in N^i_\lambda\right\}$, respectively defining the so called occlusion and transparency operations. The decomposition of images into level sets preserves their topology wrt. contrast change through $\mathbb{O}$ and $\mathbb{T}$. These operations stem from the way a natural image is formed (Blinn, 1977) (R.L.Cook and K.E.Torrance, 1982). Figures 1(a) and (c) show a sphere object O in the scene S with or without a light source. Thanks to the occlusion and transparency operations, we obtain images shown in figure 1 (b) and (d) repectively. The image intensity for each region depends straight on the characteristics of the object material, on the light source intensity and on the view point respective to the object surface and the light source direction.

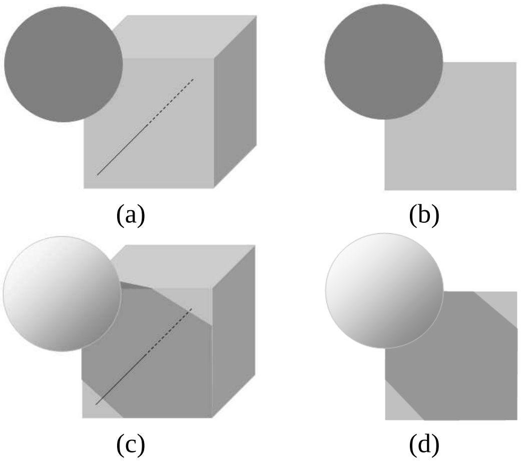

Figure 1: Image construction :(a) an object in the scene, (b) an image constructed from (a), (c) the same scene with light, (d) an image reconstructed from (c)

In the absence of more a priori information about objects and scenes in images, we assume that objects are uniform (level sets). Each level set then represents an object in a scene locally viewed as a binary image. Yet, the operation used for decompositon is unknown, then it is stated here that level sets are combined solely by the occlusion operation. Figure 2 shows an example of such decomposition.

Boundaries of level sets are called level-lines L_λ. Actually, level-lines do not exist since they are located between pixels. Objects can combine many regions but they never overlay. Level-lines from the same level set do never overlay or cross. But level-lines from different level sets can overlay of course. Let these overlayed level-lines for λ from u to v be the *level-line flow*, the flow extension $\mathcal{E}$ is then defined by $v - u$.

$$F_{u,v} = \{L_\lambda \diagup \lambda \in]u,v]\} \quad (1)$$

By construction, true occlusions between objects in the scene reflect on junctions in the image, to be further detected by the occlusion operation. These junctions are located at the point, between any four neighbour pixels, where two different level-lines merge or split. Many junctions appear or disappear from an image to the other. This phenomenon occurs with important light changes or noise. We call that type of junctions the *virtual junctions*. Their unstability comes from the fact that they originate in intensity variations wrt. the same material/surface of an object in the scene Conversely, junctions from real occlusions in the scene remain quite stable along with images. We call *real junctions* these latter consistent ones. They are actually produced by the reflectance of different materials for the same light source. That is why real junctions are invariant to contrast changes. Also, they likely correspond to a higher contrast between regions than virtual junctions'. To distinguish between real and virtual junctions, we then look for a repetition of the same junction at a point in the image (overlayed junctions). The more the more likely. From this property, real junctions thus materialize as *flow junctons* where $\mathcal{E}$ measures the repetition number. Junctions can be classified into three types : *X* junction formed by three level-line flows, *Y* junction formed by two level-line flows and *L* junction (corner) formed by one level-line flow. In section 4 we discuss

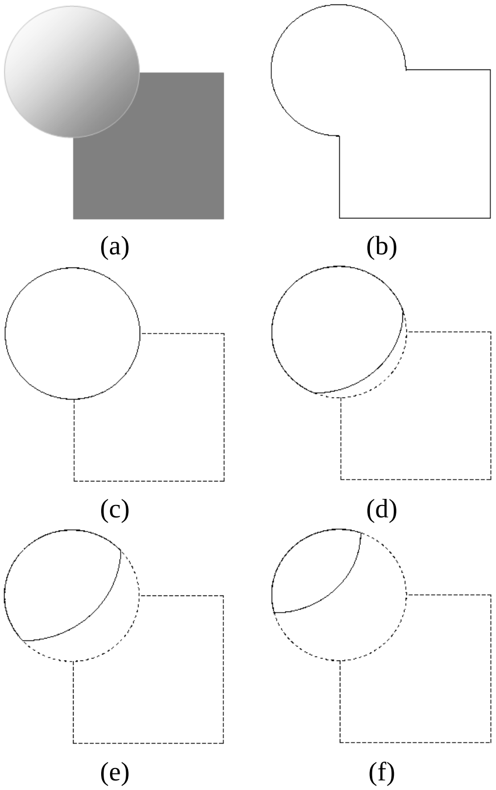

Figure 2: Image decomposition into level sets : (a) the sphere image, (b)-(f) level set with different λ

how to extract *Y* and *L* junctions. Real X junctions are rare and can be considered Y junctions anyway by ignoring the smallest flow among four (see section 4).

3 DETECTION OF POTENTIAL FLOW JUNCTIONS

When extracting flow junctions based solely on the flow extension threshold $\mathcal{E}$, results turn out to be still very sentitive to local noise. All the more as it is difficult to set an appropriate threshold for all conditions inside an image. Following the argument in the section above, $\mathcal{E}$ represents a degree of reality for a junction, and mostly virtual junctions should be sentitive to contrast changes. For a noise resistant detector, we first select potential flow junctions by measuring the variation around junction points (between any four neighbour pixels). Measures of the variation at a point were studied by many authors, since pixels around the singularity show a much higher variation than edge- or region-pixels . Moravec (Moravec, 1979) determined the variation by computing various intensity directionnal differences inside a small window and its neighbourhood. Harris (Harris and Stephens, 1988) developed a popular local operator by computing and diagonalizing the covariance of first order directionnal derivatives as an analytic image expansion within a Gaussian weighted circular window for noise reducing and extension framing. A common problem with all methods of the kind is that their response depends considerably on the constrast range. That makes it difficult to set parameters or thresholds. Additionnally many of them use a Gaussian smoothing to noise reduction that hampers junction localization as a side effect. From both main problems it did not seem adequate to adapt such methods to level lines. Completely different approaches like Girard's (Girard, 1980), the one by Bonnin and al. (Bonnin et al., 1989) or Smith and Brady's SUSAN (Smith and Brady, 1997) measure the variation in making no assumption about junction types and without any prior smoothing. The threshold is simply used as an intensity variation range limit . They assume that junctions are formed by a couple of regions having constant or near constant intensity. That makes implicitly the method limit to *L* junctions (corners). Here we propose an extension of SUSAN like methods, adapted to flow junctions tracking and improved to deal with other types of junctions.

In the classic SUSAN method, a circular mask is applied at each pixel p then one measures intensity variations between p and every other pixel within the mask. If $\mathcal{N}_p$ is the number of pixels where the variation is less than a threshold $\frac{\mathcal{E}}{2}$ and $\mathcal{N}_p$ is less than half the mask size $\mathcal{N}_m$ the center pixel is considered a potential junction with response $\mathcal{V}_p$. The area in the mask covered by these pixels is called USAN.

$$\mathcal{N}_p = \textstyle\sum_{p_i \in w} \mathcal{C}_{p_i}$$

$$\mathcal{C}_{p_i} = \begin{cases} 1 & \text{if} \quad |I(p) - I(p_i)| \leq \frac{\mathcal{E}}{2} \\ 0 & \text{else} \end{cases} \tag{2}$$

$$\mathcal{V}_p = \begin{cases} \frac{\mathcal{N}_m}{2} - \mathcal{N}_p & \text{if} \quad \mathcal{N}_p < \frac{\mathcal{N}_m}{2} \\ 0 & \text{else} \end{cases} \tag{3}$$

Adapting the idea to flow junctions, we keep the same formulas to computing $\mathcal{N}_p$ but we consider that junction points are located between any four pixels. We define the flow junction variation $\mathcal{V}^p$ as the sum of all pixel variations $\mathcal{V}_p$ around that point.

$$\mathcal{V}_p = \begin{cases} \frac{\mathcal{N}_m}{2} - \mathcal{N}_p & \text{if} \quad \frac{\mathcal{N}_m}{16} \leq \mathcal{N}_p < \frac{\mathcal{N}_m}{2} \\ 0 & \text{else} \end{cases} \tag{4}$$

$\frac{\mathcal{N}_m}{16}$ is considered as the minimum corresponding to 2 pixels out of 36 (# 22.5 degrees) similar to p. Since each pixel's variation marks an *L* junction, the total variation shows implicitly the *X* and *Y* flow junctions. The figure 3 displays an example of *Y* junction. However this summation is computed under the condition that the difference between the maximum and minimum average intensity of FLAM's area be greater than or equal to the flow extension $\mathcal{E}$ (FLAM stands for *Flow Laminating Average Milieu* and is the geometric equivalent to the Smith's USAN in the case of level lines). This difference value indicates the largest level-line flow that could pass though the junction in question. The variation at a junction point is thus defined as

$$\mathcal{V}^p = \begin{cases} \sum_{i \in [1,4]} \mathcal{V}_{p\,i}^2 & \text{if} \quad \mathcal{M}_p^+ - \mathcal{M}_p^- \geq \mathcal{E} \\ 0 & \text{else} \end{cases} \tag{5}$$

Note that the average intensity for FLAM's area $\mathcal{M}_p$ is computed as.

$$\mathcal{M}_p = \frac{\sum_{[p_i \in w / |I(p) - I(p_i)| \leq \mathcal{E}]} I(p_i)}{\mathcal{N}_p} \tag{6}$$

Then $\mathcal{M}_p^+ = \max(\mathcal{M}_{p_i} / i \in [1,4])$ and $\mathcal{M}_p^- = \min(\mathcal{M}_{p_i} / i \in [1,4]))$. The junction variation computed this way makes the *junction variation detector*.

Figure 4 makes all notations explicit on the sketch of a Y junction in the $I = f(x, y)$ space.

In the next section, we show how to track flow junctions all through the image. Successful tracking makes the actual junctions, giving rise to the acronym EFLAM that stands for Extended FLAM. Derived junctions are to be used further as primitives in a matching process.

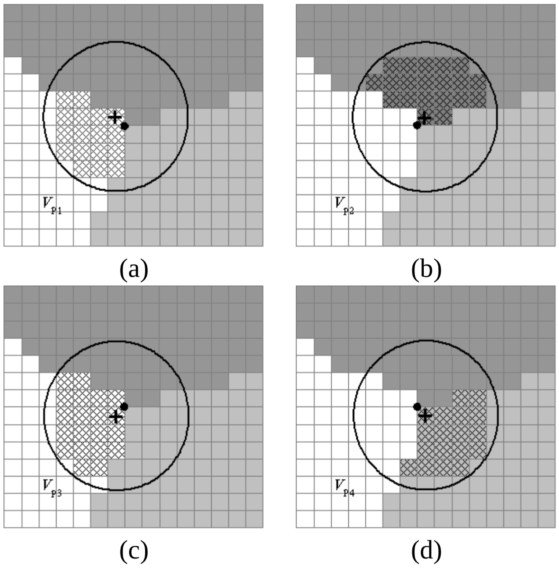

(a) (b) (c) (d)

Figure 3: FLAM area associated to four pixels around a junction point and the computed variations. (a) Variation at pixel p_1, $\mathcal{V}_{p_1}$ (b) Variation at pixel p_2, $\mathcal{V}_{p_2}$ (c) Variation at pixel p_3, $\mathcal{V}_{p_3}$ (d) Variation at pixel p_4, $\mathcal{V}_{p_4}$

4 EXTRACTION OF FLOW JUNCTIONS

Classic methods extract level-line flows in using a series of thesholds and then follow repetitive overlayed level-lines from point to point. The method is straightforward but expensive in terms of computing time. Here, we propose a tracker automaton that splits into three main steps.

First step : apply the junction variation detector. It takes an image for the input and then runs the operator at every junction point. A positive non zero value is thus attributed to any potential junction point.

Second step : track level-line flows. For every potential junction point, the automaton tracks level-line flows that form into it. To that aim, it first determines the initial flows at that point in the principal directions according to:

$$F_i = \{L_\lambda / \lambda \in]u_i, v_i]\}\ ,\ i \in [1,4] \qquad (7)$$

Where $u_i = \min(\mathcal{M}_{p_i}, \mathcal{M}_{p_{i+1(mod4)}})$ and $v_i = \max(\mathcal{M}_{p_i}, \mathcal{M}_{p_{i+1(mod4)}})$. Since only *Y* or *L* junctions are to be tracked, the antomaton deletes the least important level-line flows by comparing flow extensions $\mathcal{E}_i$. Let us underline that $\mathcal{E}_i$ can then make a control parameter for the density of junctions. Then, each valid initial flow is tracked through the image in different directions, following the conditions :

(1) the tracking flow is a subset of the destination flow,

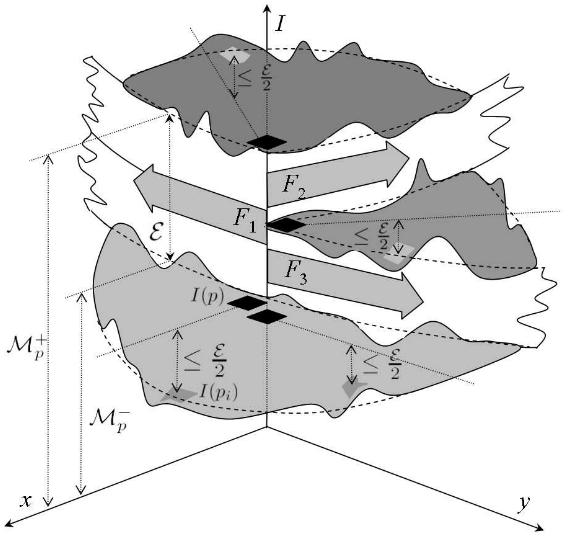
I
$\leq \frac{\mathcal{E}}{2}$
F_2
F_1
$\mathcal{E}$
$\leq \frac{\mathcal{E}}{2}$
F_3
$I(p)$
$\mathcal{M}_p^+$
$\leq \frac{\mathcal{E}}{2}$
$\leq \frac{\mathcal{E}}{2}$
$I(p_i)$
$\mathcal{M}_p^-$
x
y

Figure 4: FLAM area associated to a Y junction

(2) the tracking path will not return to its origin,

(3) the tracking path favours and preserves straight lines.

The first condition makes the automaton track the same level-line flow whatever the local image topology. Conditions (2) and (3) give best chances to important straight level-line flows in buffering. The figure 5 (a) shows an example of level-line flows tracking though a junction where $F_1 = \{L_\lambda / \lambda \in]5, 10]\}$,$F_2 = \{L_\lambda / \lambda \in]10, 20]\}$ and $F_3 = \{L_\lambda / \lambda \in]5, 20]\}$. We note that $F_1 \subset F_3$ but $F_1 \not\subseteq F_2$, and $F_2 \subset F_3$ but $F_2 \not\subseteq F_1$, by these constraints we obtain $F_a = F_2$ and $F_b = F_1$ that forms into the junction shown in figure 5(b).

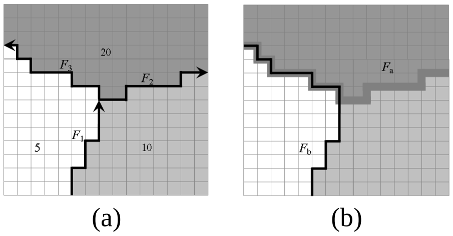

(a) (b)

Figure 5: Level-line flows tracking though a junction

Third step : code a flow junction as a primitive feature. At this step the straight level-line flow is approximated by a segment line. Its descriptors as given in equation 8 consist of the starting point, the length, the flow extension, and the average intensities left and right of the line.

$$\overrightarrow{S} = [\ \mathrm{p} \quad \mathcal{E} \quad L \quad c_l \quad c_r\ ] \qquad (8)$$

Where $c_l = \frac{\sum \mathcal{M}_{p_l}}{L}$, $c_r = \frac{\sum \mathcal{M}_{p_r}}{L}$ and $\mathcal{E} = \frac{\sum_{i<L} |\mathcal{M}_{p_{i_r}} - \mathcal{M}_{p_{i_l}}|}{L}$. The Y junction which is formed by two level-line flows is defined as aprimitive $\overrightarrow{P}$ combining three segments. Likewise the L junction can be approximated by two segments. We define the principal segment $\overrightarrow{S}_*$ of a primitive as the one supported by the maximal level-line flow among the three that join at point p in case of a Y. In case of an L it corresponds to the first detected flow along with the image scan. Virtual pixel p is the control point of the primitive to be further matched. Angles θ_l and θ_r are measured from the principal segment to respectively the one on its left $\overrightarrow{S}_l$, and the other on the right $\overrightarrow{S}_r$. The figure 6 shows the primitive associated to the Y flow junction in figure 5.

$$\overrightarrow{P} = \left[\begin{array}{cccccc} \mathrm{p} & \overrightarrow{S}_* & \overrightarrow{S}_l & \overrightarrow{S}_r & \theta_l & \theta_r \end{array} \right] \qquad (9)$$

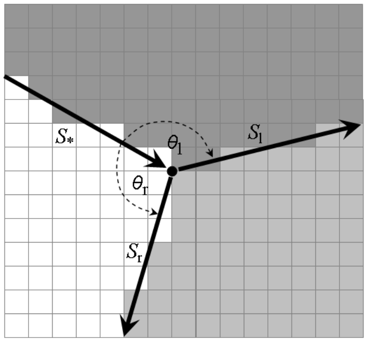

Figure 6: Definition of primitive

Note that binding the principal segment of a primitive to the actual image local configuration makes flow junctions rotation invariant. Moreover, the order of magnitude of region intensities around the junction could constrain the matching tighter.

$$\mathcal{F}_{\overrightarrow{P}} = \mathcal{V}^p \sum_{\overrightarrow{S}_i \in \overrightarrow{P}} L_i \times \mathcal{E}_i \qquad (10)$$

$\mathcal{F}_P$ appears eventually as the reliability of a primitive, to be used for non-maximum suppression in the case we extract corners or for multi-round matching when primitives would be progressively involved according to that latter reliability. Let us underline that, unlike most methods based on points of interest, no more descriptor $-$ moment, derivative, Fourier parameters etc. $-$ needs to be further computed to matching. Next section starts with comparing our results to Harris's, and then stresses upon the control of the junction scattering over an image.

5 RESULTS

The performance of our method is compared to the one by Harris on real scene images, shown in figure 7(a) ”block image” and figure 10(a) ”house image”. We select the Harris detector, not SUSAN or others, for appearing as the more dependable especially with affine transforms even if it is not the more precise or robust to noise. The best results of the Harris operator, as found in ”http://www.cim.mcgill.ca/ dparks/”, are displayed in figure 7(b) and 10(b) respectively. By applying our method with $\mathcal{E} = 10$, all junctions extracted from ”block image” before non-maximum suppression are shown in figure 9(a). Figure 9(b) displays junctions selected from figure 9(a) as local maxima by their reliability. Junction points are then superimposed in ”block image” (figure 7(c)) to compare with the Harris operator. All corners are found by EFLAM unlike with Harris as indicated by the arrows. This is to the price of more edge-like points. Our detector is more sensitive to shadows (see circled points in figure 7(c)). Yet our results are bound to the selection strategy for $\mathcal{E}$. Increasing $\mathcal{E}$ to 14 8, gets rid of shadow/edge points to the detriment of the precision of point location. Similarly, by applying the method to ”house image” all extracted junctions and sectected junctions are shown in figure 11(a) and 11(b) respectively. Results interpretation remains the same for 9(b) and (c) as for 7(b) and (c). However our miss of the upper right corner of the bright vertical window shows the criticity of $\mathcal{E}$, whence the next kind of experiments about possible loops on $\mathcal{E}$ while matching.

Indeed, another important advantage to stress upon is that we can control the spread of extracted junctions over the image. That is very important e.g. for 3D reconstruction. The extraction is performed as a repetitive process by decreasing the flow extension $\mathcal{E}$. At the beginning, junctions are extracted with a high value of $\mathcal{E}$. Then an exclusion zone is defined as a circular area around any extracted junction point. Next round, the extraction method repeats with a lesser value of $\mathcal{E}$ adding newly found junctions only in the authorized empty zones. The smaller $\mathcal{E}$, the more occuring junctions. Note that since the reliability of primitives is computed from the flow extension $\mathcal{E}$ respective to length and variation, primitives obtained early in the process are likely more reliable. That turns out to be very useful for multi-round mathcing.

Figures 12(a) and (b) show an example of ”bust” stereo images. Extracted junctions from the left and right images in the first round, where $\mathcal{E} = 20$, are shown in figure 13(a) and (b) respectively. The extracted junctions cover barely principal structures : head, eyes, mouth, and nose. Figure 13(c) and (d) show the second round of extraction, where $\mathcal{E} = 15$, adding to junctions extracted from the first round. Now junctions represent more details of the face, while being regularly organized that helps reconstruction..

6 CONCLUSION

We presented in this paper the extraction of level-line junctions. The method is based on both level-line flow and flow junction concepts. The potential flow junctions are first detected according to the EFLAM model. It computes the variation around any junction point from the FLAM's areas. The method makes extracted junctions robust to noise and contrast change. The image primitives coded from extracted junctions are rotation invariant thanks to the local image pattern. One main advantage of our method is that we can control the spread of extracted junctions over an image and that is very useful for matching in general and peculiarly 3D reconstruction.

REFERENCES

Blinn, J. F. (1977). Models of light reflection for computer synthesized pictures. *SIGGRAPH'77 Proceedings*, 11(2):192–198.

Bonnin, P., Pauchon, E., and Zavidovique, B. (July 1989). Tracking in infrared imagery based on a point of interest/region cooperative segmentation software agents activities. In *ICIP'89, 3rd International Conference on Image Processing*, Warwick. ICEIS Press.

Caselles, V., Coll, B., and Morel, J.-M. (1999). Topographic maps and local contrast changes in natural images. *Int. J. Comput. Vision*, 33(1):5–27.

Girard, M. (1980). Digital target tracking. In *NATO Group*, Aalborg, Denmark.

Harris, C. and Stephens, M. (1988). A combined corner and edge detector. In *Proceedings of The Fourth Alvey Vision Conference*, pages 147–151, Plessey Research Roke Manor, UK.

Monasse, P. and Guichard, F. (1998). Fast computation of a contrast-invariant image representation. *IEEE Trans. on Image Proc.*, 9(5):860–872.

Moravec, H. P. (1979). Visual mapping by a robot rover. In *International Joint Conference on Artificial Intelligence*, pages 598–600.

R.L.Cook and K.E.Torrance (1982). A reflectance model for computer graphics. *Transactions on Graphics*, 1(1):7–24.

Smith, S. M. and Brady, J. M. (1997). Susan - a new approach to low level image processing. *Int. J. Comput. Vision*, 23(1):45–78.

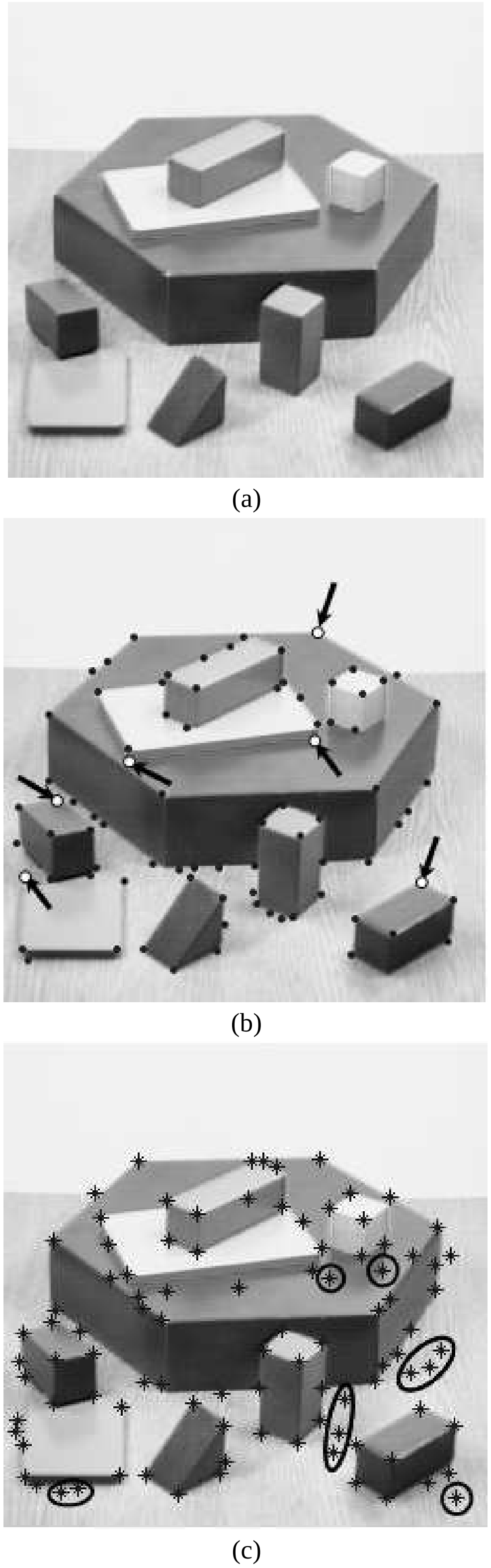

(a)

(b)

(c)

Figure 7: (a) Block test image (b) Harris corners (c) Corner by our method, $\mathcal{E} = 10$

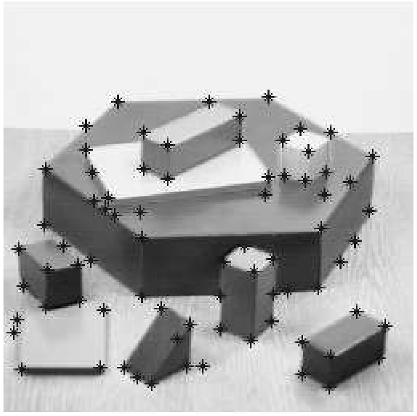

Figure 8: Trade-off between shadow-avoidance and precision for near optimal corner detection by our method, $\mathcal{E} = 14$

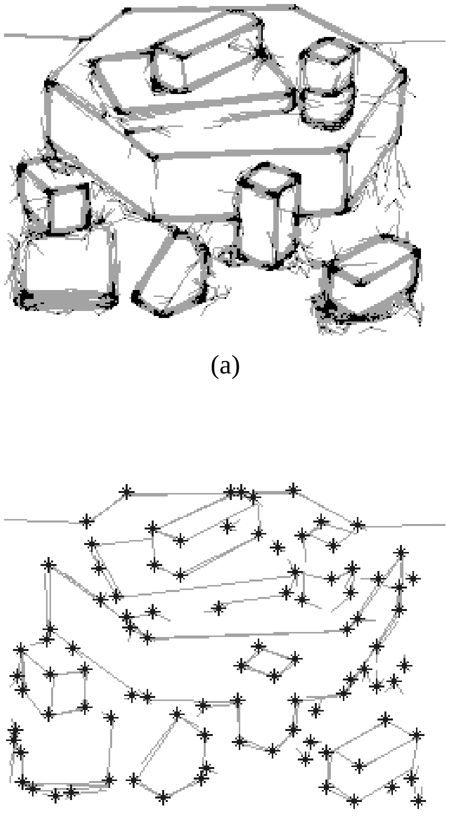

(a)

(b)

Figure 9: (a) Junctions before filtering, $\mathcal{E} = 10$ (b) Junctions after filtering, $\mathcal{E} = 10$

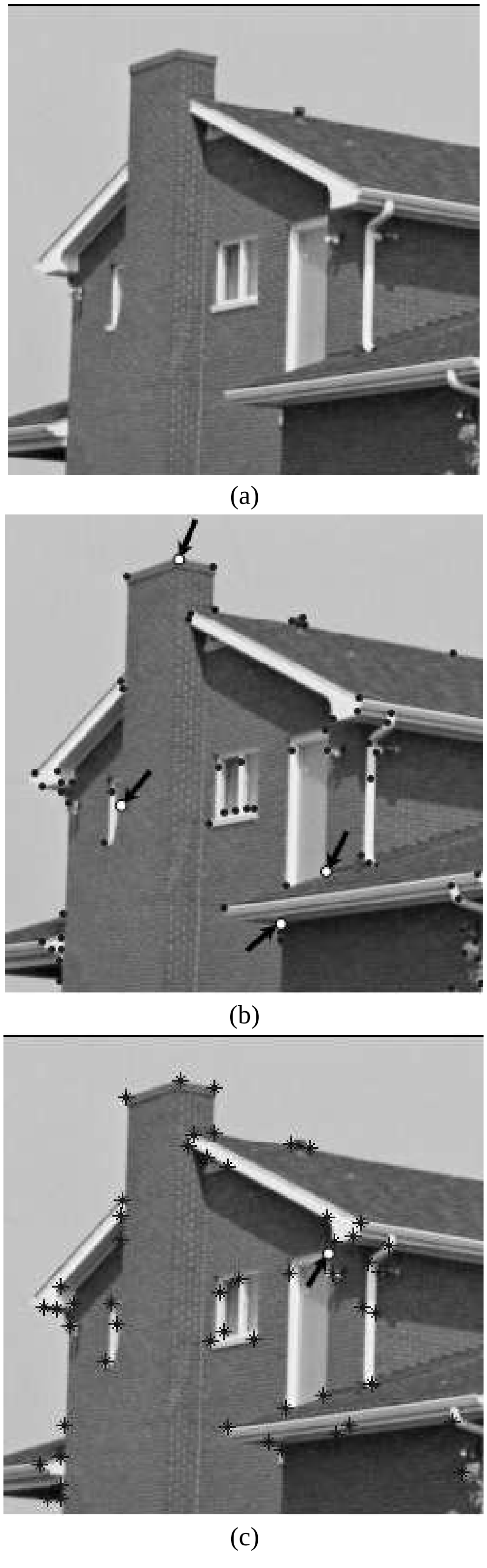

(a)

(b)

(c)

Figure 10: (a) House test image (b) Harris corners (b) Corner by our method with $\mathcal{E} = 30$

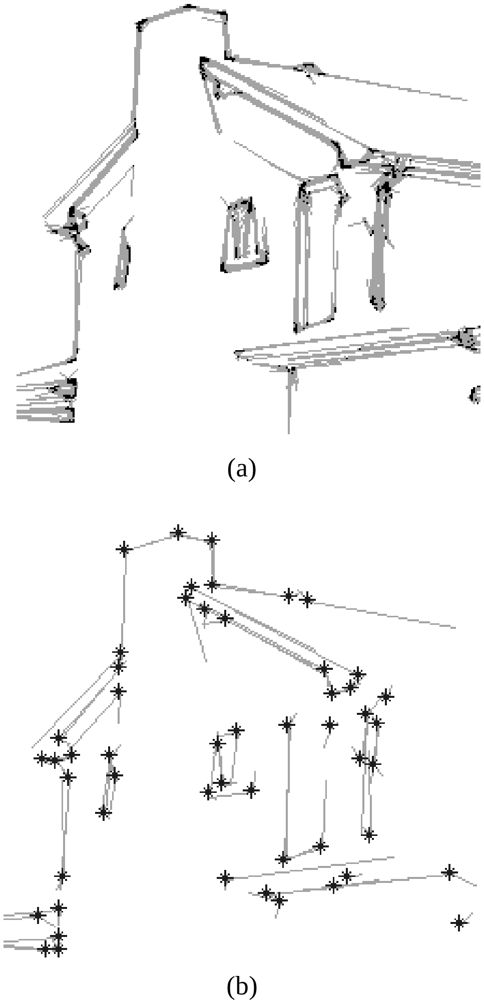
(a)

(b)

Figure 11: (a) Junctions before filtering, $\mathcal{E} = 30$ (b) Junctions after filtering, $\mathcal{E} = 30$

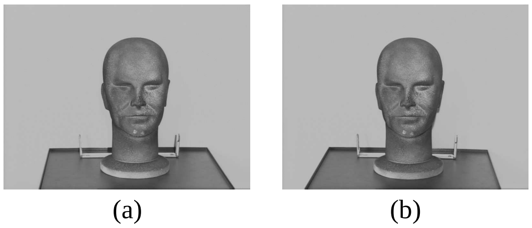
(a)

(b)

Figure 12: Stereo images (a) left image (b) right image

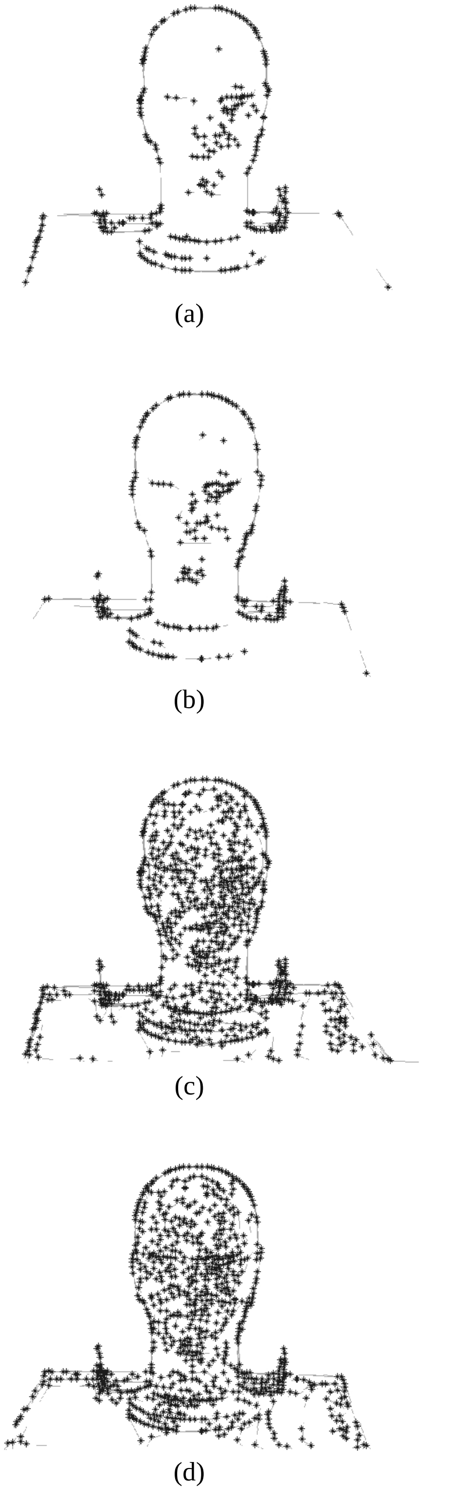
(a)

(b)

(c)

(d)

Figure 13: (a) Junctions of left image, $\mathcal{E} = 20$ (b) Junctions of right image, $\mathcal{E} = 20$ (c) Junctions of left image, $\mathcal{E} = 15$ (d) Junctions of right image, $\mathcal{E} = 15$